eNeuro

*Research Article: New Research | Novel Tools and Methods*

# Focused ultrasound neuromodulation and the confounds of intracellular electrophysiological investigation

https://doi.org/10.1523/ENEURO.0213-20.2020

**Cite as:** eNeuro 2020; 10.1523/ENEURO.0213-20.2020

Received: 22 May 2020
Revised: 14 July 2020
Accepted: 17 July 2020

**1. Title**

Focused ultrasound neuromodulation and the confounds of intracellular electrophysiological investigation

**2. Abbreviated title**

Electrophysiological issues of ultrasound studies

**3. Author names**

1. Morgan N. Collins

   Affiliation: Graduate Program in Neuroscience, University of Minnesota, St. Paul, MN 55108, USA

2. Karen A. Mesce

   Affiliation: Graduate Program in Neuroscience, University of Minnesota, St. Paul, MN 55108, USA; Departments of Entomology and Neuroscience, University of Minnesota, St. Paul, MN 55108, USA

**4. Author contributions**

MNC designed research, performed research, analyzed data and wrote the paper. KAM designed research and wrote the paper.

**5. Correspondence should be addressed to:**

mesce001@umn.edu

**6. Number of Figures:** 6

**7. Number of Tables:** 1

**8. Number of Multimedia:** 0

**9. Number of words for Abstract:** 250

**10. Number of words for Significance Statement:** 120

**11. Number of words for Introduction:** 746

**12. Number of words for Discussion:** 1082

**13. Acknowledgements**

We would like to thank Jerel Mueller, John Basile and Gerardo Rodriguez for their assistance in obtaining hydrophone characterization of the ultrasound output.

**14. Conflict of Interest**

Authors report no conflict of interest

**15. Funding sources**

This work was funded by a University of Minnesota MnDRIVE Neuromodulation Fellowship to MNC and a Grant-in-Aid of Research to KAM. This work was also partially funded by NSF grant #1451007 awarded to KAM.

**ABSTRACT**

Focused ultrasound can modulate neuronal activity noninvasively with high spatial specificity. In intact nervous systems, however, efforts to determine its enigmatic mode of efficacy have been confounded by the indirect effects of ultrasound on mechanosensitive sensory cells and the inability to target equivalent populations of cells with precision across preparations. Single-cell approaches, either via cultured mammalian neurons or tractable invertebrate neural systems, hold great promise for elucidating the cellular mechanisms underlying the actions of ultrasound. Here, we present evidence from the medicinal leech, *Hirudo verbana*, that researchers should apply caution when utilizing ultrasound in conjunction with single-cell electrophysiological recording techniques, including sharp-electrode intracellular recording. Although we found that ultrasound could elicit depolarization of the resting membrane potential of single neurons, a finding with precedent, we determined that this effect and others could be reliably mimicked via subtle manual displacement of the recording electrode. Because focused ultrasound is known to induce resonance of recording electrodes, we aimed to determine how similarly ultrasound-induced depolarizations matched those produced by micro movements of a sharp glass electrode, a phenomenon we believe can account for purported depolarizations measured in this manner. Furthermore, we show that when clonally related homologous neurons, which are essentially isopotential, are impaled prior to the application of focused ultrasound, they show a statistically significant change in their membrane potential as compared to the homologous cells that received ultrasound with no initial impalement. Future investigations into ultrasound's cellular effects should attempt to control for potential electrode resonance or utilize alternative recording strategies.

67

68 **SIGNIFICANCE STATEMENT**

69 Interest in focused ultrasound (US) neuromodulation has soared in recent years, yet
70 researchers have yet to agree on whether ultrasound excites or inhibits neuronal activity, or
71 what mechanisms underly these effects. Basic investigations have attempted to clarify how US
72 affects neuronal membrane properties to understand how it alters firing rates. Several groups
73 have linked ultrasound-induced excitation to depolarization of the resting membrane potential,
74 as measured with intracellular sharp electrodes or membrane patch methods. Here, we
75 replicate this depolarization while recording with intracellular sharp electrodes, but find that
76 the depolarizing effects of US can be replicated by small displacements of the recording
77 electrode. We conclude that intracellular electrophysiological investigations of ultrasound's
78 neuromodulatory effects are susceptible to artifacts introduced via electrode resonance.

79

80 **INTRODUCTION**

81 Focused ultrasound (US) is currently under investigation as a promising noninvasive
82 neuromodulation technology. Reports of the effects of US on nervous tissue date back 100
83 years (Harvey, 1929). Recently, the pace of US neuromodulation research has accelerated as
84 other neuromodulatory technologies (e.g., those utilizing implantable devices) have proven to
85 be therapeutic for the treatment of an ever-increasing array of neurological disorders. Uniquely
86 among noninvasive technologies, US has the ability to deliver energy noninvasively to deep
87 brain structures with high spatial specificity (Hynynen and Clement, 2007; Ai et al., 2016).

88

Despite evidence that US modulates neuronal activity in a wide range of animal systems, including humans (Legon et al., 2014, 2018), inconsistencies in reported outcomes persist with respect to the direction of its effects. Researchers have reported both US-induced neuronal excitation (e.g., Tyler et al., 2008; Tufail et al., 2010; Yoo et al., 2011; Kim et al., 2012, 2014; Downs et al., 2018) and inhibition (Fry et al., 1958; Rinaldi et al., 1991; Min et al., 2011; Legon et al., 2014, 2018; Kim et al., 2015). Furthermore, underlying mechanisms to account for the neuronal excitatory and inhibitory actions of US have been ascribed to being thermal (Lele, 1963; Colucci et al., 2009; Darrow et al., 2019), mechanical (direct or via US-induced cavitation) (Plaksin et al., 2014; Wright et al., 2017; Kubanek et al., 2018; Menz et al., 2019), or a combination of the two (Bachtold et al., 1998). Efforts to elucidate how US modulates neural activity have been confounded by the US activation of mechanosensory structures, including auditory hair cells (Guo et al., 2018; Sato et al., 2018). To circumvent these and other complicating factors, we and other groups have examined how US influences neurons on a foundational level in tractable invertebrate systems (Wright et al., 2015, 2017; Yoo et al., 2017; Kubanek et al., 2018; Dedola et al., 2020), mammalian cell culture (Muratore et al., 2009; Qiu et al., 2019), or slice (Rinaldi et al., 1991; Bachtold et al., 1998; Tyler et al., 2008; Prieto et al., 2018).

Recently, we obtained evidence to support the idea that the direct effects of US on nerves at low intensities are largely inhibitory (Mesce and Newhoff, 2020; M. N. Collins, W. Legon and K. A. Mesce, unpublished observations). We obtained these results by studying a synaptically-isolated identified motoneuron in the well-studied medicinal leech, *Hirudo verbana*. This work

111 stands in contrast to some other single-cell reports whereby US was found to induce neuronal
112 excitation via depolarization of the resting membrane potential (Tyler et al., 2008; Lin et al.,
113 2019; Dedola et al., 2020). Because we used extracellular suction electrodes versus intracellular
114 or patch electrodes to record action potentials from the axons of our identified neuron, we
115 considered whether different recording methodologies might contribute to a phenomenon of
116 excitation versus inhibition.
117
118 Here, we examined the effects of US on the resting membrane potentials of identified leech
119 neurons, and asked whether the actions of US could be influenced by the impalement of a
120 sharp-glass electrode. As in vertebrate neurons, the rising and falling phases of its action
121 potential are mediated by voltage-gated sodium and potassium channels, respectively
122 (Kleinhaus, 1976; Kleinhaus and Prichard, 1976). This is important to note, as these channels
123 have been implicated as actuators of US-induced neuromodulation, yet are not present in all
124 animal models under investigation with US (e.g., *C. elegans* lacks voltage-gated sodium
125 channels).
126
127 As our primary target, we chose the Retzius neuron, a serotonergic bilaterally-paired cell
128 located on the ventral surface of all 21 segmental ganglia. This cell has been extensively studied
129 since its discovery in 1891 (Carretta, 1988). Its large soma (50-80 μm diameter) has enabled its
130 rapid identification and subsequent impalement during intracellular recording experiments. The
131 two Retzius neurons per segmental ganglion are electrotonically coupled and nearly
132 isopotential (Hagiwara and Morita, 1962; Eckert, 1963). To compare our findings with a recent

intracellular investigation of US on leech nociceptive (N) cells (Dedola et al., 2020), we performed additional experiments on this cell type.

Specifically, we studied whether physical microadjustments of the intracellular electrode could mimic the depolarized state and related action potential parameters induced by US. We found that US-induced changes, including depolarization of the resting membrane potential, an increase in spike frequency, and attenuation of spike amplitude could be mimicked by brief, manual electrode displacements. Due to known US-induced electrode resonance, the rapid depolarization of cells found to occur in neurons in response to US application during intracellular recording may be artifactual, as we have found here.

## MATERIALS AND METHODS

### Animal preparation

We examined the effects of US and manual electrode displacement on Retzius neurons from the medicinal leech, *Hirudo verbana*. Retzius cells are present bilaterally in each of the leech's 21 segmental ganglia; a diagram of the leech nervous system and a single ganglion are shown in Fig. 1a & b. Retzius cells can be readily identified due to their large size and firing properties, enabling rapid entry and re-entry of the same cell. The resting membrane potential is typically -30 to -50 mV, and spikes are 20 to 50 mV in amplitude (Hagiwara and Morita, 1962; Eckert, 1963). The cell's soma and neurites are visible in a Neurobiotin cell fill in Fig. 1c.

We obtained hermaphroditic adult leeches from Niagara Medical Leeches (Niagara, NY, USA); they were housed at room temperature (22-24°C) in a large tank filled with pond water and anaesthetized on ice prior to dissection. Single leech ganglia were pinned ventral side up in a petri dish lined with 2 mm-thick SYLGARD™ (Dow Corning) and filled with leech saline (in mM: 115 NaCl, 4.0 KCl, 1.8 $CaCl_2$, 1.5 $MgCl_2$, 10.0 Glucose, and 10.0 Trizma pre-set crystals, all from Sigma Aldrich; recipe adapted from Nicholls and Baylor, 1968). A 5 mm diameter circle of SYLGARD™ directly beneath the ganglion was removed, and the hole in the dish was sealed with a thin layer of latex.

**Intracellular recording**

The somata of Retzius neurons were impaled with sharp electrodes made from borosilicate glass (1 mm outer diameter, 0.75 mm inner diameter) pulled to resistances of 25-40 MΩ on a micropipette puller (P-87, Sutter Instrument Co.); electrodes were filled with 2 M potassium acetate and 20 mM KCl (Cymbalyuk et al., 2002). Recordings were amplified (IX2-700 dual intracellular preamp, Dagan Corp.), digitized (Axon CNS Digidata 1440A, Molecular Devices), and bridge balanced. Data were acquired with pClamp software (Axon Instruments) and imported into MATLAB (R2018b, MathWorks, Inc.) for analysis.

The ultrasound transducer (Sonic Concepts H102-MR) was placed beneath the preparation (see schematic in Fig. 1d). The degassed, deionized water-filled focusing cone was sealed to the latex-covered dish opening with a drop of water, ensuring continuous transmission of energy from the transducer to the ganglion.

**Neurobiotin cell filling**

The Retzius cell fill displayed in Fig. 1c was filled by iontophoretic injection of Neurobiotin (Vector Laboratories). Briefly, the tip of an intracellular recording electrode was filled with 5% Neurobiotin dissolved in 2 M KAc; the electrode was then backfilled with 2 M KAc and 20 mM KCl. Following cell impalement, we injected 2 nA negative current for a duration of 20 minutes. The ganglion was incubated at room temperature for 45 minutes following iontophoretic injection to allow the dye to diffuse to distal structures. Following this incubation period, the ganglion was fixed in 4% paraformaldehyde (overnight at 4°C) and rinsed in iso-osmotic Millonig's buffer (all components from Sigma Aldrich, recipe from Puhl and Bigelow et al., 2018). Cells were permeabilized in 1% Triton in iso-osmotic buffer for 2 hours, and incubated overnight at 4°C in a 1:50 dilution of streptavidin conjugated to Cy3 (Jackson ImmunoResearch Laboratories, Inc.). The ganglion was then rinsed in iso-osmotic Millonig's buffer, dehydrated in ethanol, and mounted between glass coverslips using DEPEX mounting medium (VWR International). The filled Retzius cell was imaged on a Nikon A1 laser-scanning confocal microscope, and the resulting image was processed in ImageJ.

**Electrode displacement paradigm**

For our electrode displacement paradigm (Fig. 1e), we rapidly raised and lowered the recording electrode by rotating the knob of our micromanipulator (Leitz joystick model, Leica Optical). Distance raised was tracked using marked notches on the fine-adjustment knob (each notch corresponds to a distance of 200 nm). The motion took ca. 2 seconds, the fastest time in which

198 we could consistently raise and lower the electrode. As with our US trials, electrode
199 displacement was induced following a 20 second baseline recording, and subsequent trials had
200 increased displacement until electrode impalement was lost.
201
202 **Ultrasound characterization and parameters**
203 All US waveforms were designed by a waveform generator (Agilent 33500B Series) and
204 triggered by a TTL pulse from our intracellular recording digitizer via pClamp software.
205 Waveforms were amplified by a 100 W RF linear power amplifier (E&I, model 2100L) and
206 impedance matched with a matching network (Sonic Concepts). Transducer output was
207 characterized by hydrophone (ONDA HNR-0500) measurements in 0.5 mm increments in x, y,
208 and z directions in a large tank filled with deionized, degassed water. Shown in Fig. 2c are the
209 vertical and horizontal cross-sections of linearly interpolated hydrophone measurements (step
210 size = 500 microns in x, y, and z directions; 309 total measurements) at peak amplitudes, which
211 are overlaid with scaled preparation dimensions.
212
213 In our first paradigm (Figs. 3 & 4), US trials consisted of the application of a single tone of 960
214 kHz pulsed ultrasound for 100 ms following a 20 second baseline recording period. Pulses were
215 313 μs in duration and were delivered at a 1 kHz pulse repetition frequency. Peak pressures and
216 intensities were increased sequentially in repeated trials until the electrode impalement was
217 lost. Pulse parameters and the range of pressures and intensities used are described in Fig. 2.
218

In our second paradigm (Fig. 5), US trials consisted of a single tone of 960 kHz continuous (100% duty cycle) US applied for 300 ms. Peak pressures and intensities were increased sequentially in repeated trials until electrode impalement was lost.

In our third paradigm (Fig. 6), US trials consisted of a 20-minute application of 960 kHz pulsed ultrasound preceded by a baseline recording period of at least 20 seconds. A subsequent baseline recording was made after the ultrasound application. Ultrasound was applied for the first 10 seconds of every minute (tone duration = 10 s). Tones consisted of 313 µs pulses (pulse duration) pulsed at 1 kHz (pulse repetition frequency), yielding a duty cycle of ~30%. Ultrasound intensity and pressure were fixed at 4 W/cm$^2$ spatial peak pulse average intensity ($I_{SPPA}$) and 111 kPa, respectively.

**Statistics**

All statistical tests save power analyses were performed in MATLAB. Data were tested for normality via Shapiro-Wilk tests. Comparisons of non-normally distributed data were performed via non-parametric Wilcoxon rank-sum tests; normally distributed data were compared via Welch's *t*-tests. All hypothesis tests were two-tailed with $\alpha = 0.05$. We quantified effect sizes [Cohen's d with correction for small sample sizes (Durlak, 2009)], and performed post-hoc power analyses. Power analyses were performed using G*Power 3.1 (Erdfelder et al., 2009). All statistical results are reported in Table 1.

**Table 1**

241

| | Data Structure | Type of test | Result | Effect size | Power |
|---|---|---|---|---|---|
| a | Non-normal<br>US condition:<br>W(11) = 0.7185, p= 0.0018<br>ED condition:<br>W(11) = 0.6417, p= 4.38e-04 | Wilcoxon rank-sum test | Z= 2.6275, p=0.0086 | d = 1.3018 | 0.8438 |
| b | Non-normal<br>US condition:<br>W(9) = 0.7890, p= 0.0141<br>ED condition:<br>W(9) = 0.5623, p= 2.6799e-04 | Wilcoxon rank-sum test | Z= 0.1890, p= 0.8501 | d = 0.0135 | 0.0501 |
| c | Normal<br>US condition:<br>W(9) = 0.9659 , p= 0.8508<br>ED condition:<br>W(9) = 0.9713 p= 0.9027 | Welch's *t*-test | t(17.3329) = 0.2777, p = 0.7845 | d = 0.0343 | 0.0506 |
| d | Non-normal<br>US condition: | Wilcoxon rank-sum test | Z=100, p=1.554E-4 | d = 3.613 | 0.99 |

| | | | | | |
|---|---|---|---|---|---|
| | W(7) = 0.8499, p=0.0951 Control condition: W(7) = 0.9543 p=0.7547 | | | | |
| e | Non-normal US condition: W(7) = 0.8802, p=0.189 Control condition: W(7) = 0.8802, p=0.0274 | Wilcoxon rank-sum test | p=0.1605 | d = 1.3432 | 0.68 |

## RESULTS

### Ultrasound depolarizes Retzius neurons and alters spike frequency and waveform

For the first set of experiments, depicted in Figs. 3 and 4, we applied US as described to 14 leech ganglia while recording intracellularly from one of the bilateral Retzius cells (n = 14 Retzius cells). Data from 2/14 recordings were not included in analyses due to an unstable baseline (membrane potential rising rapidly prior to US application due to poor electrode impalement); final n = 12. US induced a dose-dependent rise in the resting membrane potential, with higher pressures yielding greater depolarization. As US pressure increased in subsequent trials, neurons typically showed increasing levels of depolarization until the cell was lost, as evidenced by a sharp, high amplitude increase in voltage consistent with partial or full

loss of electrode impalement. Aggregated data demonstrating mean depolarization at ascending pressures are shown in Fig. 3a; only data from the five lowest pressures are displayed, as these were sufficient to induce effects and/or loss in most of the cells tested, and thus our sample sizes at higher pressures were low. Responses were highly variable with respect to the pressures at which cells were lost (mean = 110.38 kPa, SD = 56.22). The mean time to peak depolarization following the US onset was 1.19 s (SD = 1.43). At maximally depolarizing pressures prior to loss (mean = 77.69 kPa, SD = 51.54), cells were depolarized by an average of 3.73 mV (SD = 3.25). We also observed changes in spike amplitude and spike frequency during peak depolarization (time from stimulus onset to beginning of a sustained period of repolarization towards baseline membrane potential). During peak depolarizations, most cells (n = 10/12) fired action potentials. Of these cells, mean spike amplitude (normalized to spike amplitude during 20 s baseline) was decreased (mean normalized spike amplitude = 0.88, SD = 0.20). Because changes in spike frequency were highly variable and the data were skewed, we have opted to report data dispersion versus mean and standard deviation. The median normalized spike frequency during the period of peak depolarization was 2.28; the interquartile range was 10.4. All data points are visible in Fig. 4b.

Despite our awareness of others achieving similar results with respect to US-induced depolarization (Dedola et al., 2020), several factors gave us pause with respect to the legitimacy of our data. First, we observed high variability in responses to our tested pressures, which was less expected in this system than others due to our use of the same identified neuron in all preparations. Second, The sharp upward deflections in membrane potential even during

moderate US-induced depolarizations were reminiscent of what we observed when a cell recording was naturally lost due to stochastic factors, a phenomenon that can occur in gradations (partial versus full loss), with a clear reduction in spike amplitude in instances in which partial electrode impalement remains. US causes mechanical disturbance of targeted tissue and can cause electrode resonance that can result in loss of contact with the recorded neuron (Tyler et al., 2008). We, like others, attributed cell loss resulting from US application to electrode resonance. We further suspected that US applications that fell below the pressure threshold to induce a full recording loss might induce a partial one, resulting in depolarization of the resting membrane potential and other reversible changes that, in isolation, could appear to be the cellular signatures of excitatory neuromodulatory processes.

**Electrode displacement mimics ultrasound-induced effects**

To determine whether brief disruption of electrode placement could elicit effects comparable to US reliably, we performed trials in which we manually displaced the recording electrode in increasing increments while recording from Retzius cells in an additional 13 ganglia (n = 13 Retzius cells). The recording electrode was raised and lowered vertically in 2-second motions; displacement magnitude was standardized via notches on the micromanipulator knob corresponding to 200 nm distances. Data from one cell was not included in analyses due to an unstable baseline (final n = 12). Increasing displacements yielded dose-dependent depolarizations (see means of data aggregated across cells in Fig. 3a.). We observed high variability in the displacement magnitude necessary to lose cell impalement, with a mean of 3.93 μm (SD = 1.92). Time to maximum depolarization was also variable, occurring on average

298 4.34s (SD = 5.83) from the start of the displacement motion. At maximally depolarizing
299 displacements, prior to cell loss (mean = 2.38 µm, SD = 1.42), cells depolarized by an average of
300 3.62 mV (SD = 2.53). We also observed a reduction in spike amplitude and a reduction in spike
301 frequency in the 10/12 cells that fired action potentials during the period of peak
302 depolarization, similar to what we had observed with US. Mean normalized spike amplitude
303 during peak US effects was 0.91 mV (SD = 0.16). Comparable to changes in spike frequency in
304 the US condition, changes were highly variable and skewed, so we again opted to describe data
305 dispersion versus mean and standard deviation. The median normalized spike frequency during
306 the period of peak depolarization was 2.24; the interquartile range was 3.23. All data points are
307 visible in Fig. 4b.
308
309 Both US and manual electrode displacement were found to depolarize cells up to a threshold
310 that resulted in a loss of the intracellular recording; examples may be seen in Fig. 3b., in which
311 traces show typical outcomes in a cell exposed to US at increasing pressures (upper; pink), and
312 a cell subjected to electrode displacement (lower; green). Time to peak depolarization differed
313 between the two conditions (see Fig. 3c and d); Z= 2.6275, p=0.0086[a]. This difference is
314 consistent with the differential in stimulus application time (100 ms for US vs. 2 seconds for
315 electrode displacement). We observed an increase in spike frequency and a decrease in spike
316 amplitude in both US and electrode displacement conditions (Fig. 4a-d). Mean increase in spike
317 frequency and decrease in spike amplitude at maximally depolarizing levels prior to loss did not
318 differ significantly between US and electrode displacement (spike frequency: Z = 0.1890, p =

319 0.8501[b], Wilcoxon rank-sum test; spike amplitude: t(17.33) = 0.2777, p = 0.7843[c], Welch's *t*-
320 test).
321
322 **The depolarizing effects of ultrasound and electrode displacement are common to**
323 **nociceptive neurons**
324 To assess whether our observed effects were applicable to other identified neurons in the
325 leech, we performed an additional set of experiments on another cell type, the nociceptive (N)
326 cell (Fig. 5a.). This cell was chosen due to its usage in a recent study in which US is reported to
327 depolarize leech neurons in an intracellular paradigm (Dedola et al., 2020). We adjusted pulse
328 parameters to mimic more closely those found to be effective in eliciting a response in N cells:
329 we applied a single pulse of continuous US with a 300 ms pulse duration (Fig. 5b). We were
330 unable to replicate fully the authors' paradigm as we were constrained by the higher center
331 frequency of our ultrasound transducer (960 kHz vs. 490 kHz).
332
333 We applied US at ascending pressures to 6 N cells (n = 6) while recording intracellularly. Our
334 first tested pressure was 20 kPa (root mean squared, the highest pressure used by Dedola et al.
335 (2020)); we observed that 0/6 cells responded. Increasing pressures, however, were sufficient
336 to elicit depolarization and, ultimately, loss of electrode impalement. At maximally depolarizing
337 pressures prior to recording loss (mean = 49.3 kPa, SD = 30.5), mean depolarization was 3.50
338 mV (SD = 4.11). A representative trace of this depolarization is displayed in Fig. 5c (upper).
339

We next assessed whether these effects could be mimicked by electrode displacement in a manner comparable to what we observed in Retzius cells. We again displaced the recording electrodes by ascending distances until the intracellular recording was lost. We observed a similar phenomenon, in which electrode deflections insufficient to compromise the recording resulted in small depolarizations. Maximal depolarization prior to loss of electrode impalement was achieved at 2.25 μm (SD = 0.99), and averaged 3.45 mV (SD = 3.45). A representative trace of this effect is displayed in Fig. 5c (lower).

**Ultrasound application following electrode impalement depolarizes Retzius neurons**

Our results in both cell types raised concern as to whether US-induced changes in the resting membrane potential of neurons could be accurately assessed via intracellular recording during US application. We next sought to determine whether it was feasible to measure changes by comparing baseline characteristics from the same cell before and after ultrasound application. The large, physiologically robust, and easily identifiable nature of the Retzius neurons enabled re-entry into the same cell in 20-30 seconds following cessation of US application. We were concerned that the effects of a 100 ms application of pulsed US, as we had used in our previous experiment, would not persist for the time taken to re-enter the cell. Assuming longer application times yielded more persistent effects, we dramatically increased the US application period to 20 minutes. Ultrasound parameters for these experiments are outlined in Fig. 6a.; the broader experimental design is outlined in Fig. 6b.

We found that Retzius neurons (n = 8) exposed to 20 minutes of ultrasound were depolarized from their pre-US baseline (mean change = 16.03 mV, SD = 8.29). Neurons re-entered after a 20-minute wait period with no ultrasound (control condition, n = 8) did not have a demonstrable change in membrane potential (mean change = 0.0625 mV, SD = 5.57). The change in membrane potential in the US vs. control conditions differed significantly (Z=100, p=1.554E-4[d], Wilcoxon rank-sum test). Intracellular traces recorded in the same cell before and after US application are shown for comparison in Fig. 6c.

Despite this compelling result, we were concerned that the depolarization we observed as a function of US application could still have resulted from electrode-associated artifactual effects, including creation of a leaking puncture in the cell membrane, or the introduction of cavitational nuclei. As a control, we performed a similar experiment in which we recorded from the contralateral Retzius neuron following US application instead of the same cell (see schematic in Fig. 6b, lower). The two Retzius neurons in each ganglion are electrically coupled and are known to be isopotential (Hagiwara and Morita, 1962; Eckert, 1963). Recording from the contralateral cell yielded an opportunity to estimate changes in membrane potential caused by US in an electrode-naïve cell. Intriguingly, the depolarization we observed in the same-cell condition did not persist significantly in the contralateral condition (p = 0.1605, Wilcoxon rank-sum test), suggesting the stark depolarization we observed in the same-cell condition could have been influenced by the initial electrode impalement.

## DISCUSSION

**Overview**

We have demonstrated that US reliably produces a dose-dependent depolarization of the resting membrane potential of single leech Retzius neurons when applied during intracellular sharp-electrode recording. We found that these effects, however, are likely to be artifactual as they could be mimicked by the manual displacement of the recording electrode. US effects appeared to differ from manual electrode displacement only with respect to the time to achieve peak effects. We believe that this difference is simply due to the time course of the applied stimulus across the two paradigms; for example, US was delivered for 100 ms, while manual displacement and replacement of the electrode took longer (ca. 2 seconds). We also determined that even when the recording electrode was removed from the targeted neuron during US application, the baseline (i.e., first) impalement appeared to cause a sufficient leak current to affect the subsequent membrane properties of the Retzius cell when recorded after US application (Fig. 6). In contrast, by recording from the electrode-naïve contralateral Retzius neuron, which was impaled only once and after the US was applied, we observed that US did not induce a statistically significant elevation in resting membrane potential.

We observed similar results, as discussed above, when targeting N cells, sensory neurons recently reported to depolarize during US application (Dedola et al., 2020). Utilizing one of the authors' employed pulse parameters (300 ms of continuous US), we observed depolarization of a comparable magnitude. Achieving this effect, however, required the use of higher pressures than the authors reported, which we attribute to our use of a higher US frequency. Higher frequencies (with lower wavelengths) generate less electrode resonance. As we suspect that

405 electrode resonance is a primary driver of depolarization in intracellular paradigms, it follows
406 that higher pressures may be required to elicit comparable depolarizations when working with
407 higher US frequencies. Importantly, by briefly displacing the recording electrode, we were able
408 to mimic the effects of US on the N cells as well.
409
410 We conclude that a nonspecific leak current most likely contributes to the US-induced
411 depolarizations we observed. In leech neurons, it has been shown previously that sharp
412 electrode impalement can affect nonspecific leak currents, having profound effects on the
413 ability of some cells, for example, to exhibit endogenous bursting activity (Cymbalyuk et al.,
414 2002).
415
416 **The confounds of electrode recording techniques**
417 Ultrasound-induced electrode resonance is a commonly-reported problem, complicating efforts
418 to asses US effects via whole-cell patch clamp (Tyler et al., 2008; Prieto et al., 2018) and two-
419 electrode voltage clamp (Kubanek et al., 2016). Although these reports utilized different single-
420 cell recording modalities, some of the electrophysiological signatures of neuromodulation
421 following US onset resemble our own, characterized by a very steep initial depolarization that
422 elicits action potentials (Tyler et al., 2008). This steep depolarization and increase in spike
423 frequency were observed similarly in a recent intracellular sharp electrode study of the actions
424 of US on a type of leech sensory neuron (Dedola et al., 2020). These authors also reported a US-
425 associated reduction in spike amplitude, which is consistent with our US and electrode
426 displacement data. We cannot rule out the possibility that US can induce a rapid depolarization,

427 at certain US parameters and in some types of neurons across animal models, as suggested by
428 prior work utilizing optophysiological techniques (Tyler et al., 2008; Qiu et al., 2019). We can,
429 however, strongly posit that electrode resonance is a potent indirect driver of US-induced
430 neuronal stimulation in the context of intracellular paradigms, especially in the leech.
431
432 Concerns of artifactual effects have been raised previously, when it was postulated that US-
433 induced electrode resonance, particularly at sub-MHz frequencies, could introduce depolarizing
434 leak currents in *Xenopus* oocytes (Kubanek et al., 2016). It remains unclear whether
435 extracellular recordings are similarly prone to artifactual effects when combined with US.
436 Minute movements of an animal preparation or displacement of any type of electrode induced
437 by ultrasound could cause a temporary reduction in electrode resistance, yielding an artifactual
438 reduction in voltage as measured, for example, in the form of a reduced-amplitude single or
439 compound action potential.
440
441 One additional concern in combining US with single-cell electrophysiological recording
442 techniques is the potential to introduce cavitational nuclei. Ultrasound has been theorized to
443 depolarize neurons through the rhythmic expansion and contraction of microbubbles in the cell
444 membrane, altering membrane capacitance (Krasovitski et al., 2011; Plaksin et al., 2014).
445 Electrode insertion could transport non-endogenous cavitational nuclei to the cell membrane
446 from the surrounding media, facilitating US effects. Degassing the saline medium, as was done
447 in our report, may limit the potential for artifactual cavitational effects. However, aerating bath
448 disturbances caused by insertion and movement of the recording electrode remain potential

449 considerations. The introduction of cavitational nuclei may be of particular concern with
450 mammalian preparations that require continued oxygenation.
451
452 **Alternative approaches**
453 Moving forward, reducing the confounds of electrode resonance will be important to achieve
454 confidence in defining the cellular underpinnings of ultrasound's actions. Resonance can be
455 reduced by separating the recording site from the site of US application (e.g., applying US to a
456 neuron's axon while recording from the soma). This is an imperfect solution, however, as distal
457 changes to membrane properties may not be accurately reflected at the soma due to space
458 clamp issues (Spruston and Johnston, 2008). Another potential means of reducing resonance is
459 by increasing US frequency, thereby decreasing wavelength, a strategy with which other groups
460 have found success (Prieto et al., 2018; Ye et al., 2018). Although this latter strategy may be
461 effective in reducing resonance, it cannot eliminate it entirely, and there remains the potential
462 for a resonating electrode to cause a leak at the site of electrode entry, increasing cell
463 permeability to surrounding sodium-rich media and inducing artifactual depolarization. In
464 addition, it remains unclear whether US at frequencies in the 10s of MHz range, as used in
465 these studies, affect neural function in a manner comparable to US in the 100s of kHz range
466 utilized in transcranial studies (e.g., Tufail et al., 2010; Min et al., 2011; Legon et al., 2014, 2018;
467 Lee et al., 2016).
468
469 In conclusion, we are of the opinion that future investigations exploring the effects of US on
470 single neurons should avoid simultaneous intracellular recording and ultrasound delivery.

Investigations that incorporate extracellular or optical recording approaches may be better suited to control for the potential artifactual effects of electrode resonance, an idea already adopted by some other groups who have found success with optical alternatives to classical electrophysiological techniques, including the use of ion-indicator dyes (Tyler et al., 2008; Qiu et al., 2019).

478 **References**

479 Ai L, Mueller JK, Grant A, Eryaman Y, Legon W (2016) Transcranial focused ultrasound for BOLD
480 fMRI signal modulation in humans. Conf Proc IEEE Eng Med Biol Soc:1758–1761.
481 Bachtold MR, Rinaldi PC, Jones JP, Reines F, Price LR (1998) Focused ultrasound modifications of
482 neural circuit activity in a mammalian brain. Ultrasound Med Biol 24:557–565.
483 Carretta M (1988) The retzius cells in the leech: A review of their properties and synaptic
484 connections. Comp Biochem Physiol -- Part A Physiol 91:405–413.
485 Colucci V, Strichartz G, Jolesz F, Vykhodtseva N, Hynynen K (2009) Focused ultrasound effects
486 on nerve action potential in vitro. Ultrasound Med Biol 35:1737–1747.
487 Cymbalyuk GS, Gaudry Q, Masino MA, Calabrese RL (2002) Bursting in leech heart interneurons:
488 Cell-autonomous and network-based mechanisms. J Neurosci 22:10580–10592.
489 Darrow DP, O'Brien P, Richner TJ, Netoff TI, Ebbini ES (2019) Reversible neuroinhibition by
490 focused ultrasound is mediated by a thermal mechanism. Brain Stimul 12:1439–1447.
491 Dedola F, Severino FPU, Meneghetti N, Lemaire T, Cafarelli A, Ricotti L, Menciassi A, Cutrone A,
492 Mazzoni A, Micera S (2020) Ultrasound stimulations induce prolonged depolarization and
493 fast action potentials in leech neurons. IEEE Open J Eng Med Biol 1:23–32.
494 Downs ME, Lee SA, Yang G, Kim S, Wang Q, Konofagou EE (2018) Non-invasive peripheral nerve
495 stimulation via focused ultrasound in vivo. Phys Med Biol 63:035011.
496 Durlak JA (2009) How to select, calculate, and interpret effect sizes. J Pediatr Psychol 39:917-
497 928.
498 Eckert R (1963) Electrical interaction of paired ganglion cells in the leech. J Gen Physiol 46:573–
499 587.

500 Erdfelder E, FAul F, Buchner A, Lang AG (2009) Statistical power analyses using G*Power 3.1:
501 Tests for correlation and regression analyses. Behav Res Methods 41:1149-1160.
502 Fry FJ, Ades HW, Fry WJ (1958) Production of reversible changes in the central nervous system
503 by ultrasound. Science 127:83–84.
504 Guo H, Hamilton M, Offutt SJ, Gloeckner CD, Li T, Kim Y, Legon W, Alford JK, Lim HH (2018)
505 Ultrasound produces extensive brain activation via a cochlear pathway. Neuron 98:1020-
506 1030.
507 Hagiwara S, Morita H (1962) Electrotonic transmission between two nerve cells in leech
508 ganglion. J Neurophysiol 25:721–731.
509 Harvey EN (1929) The effect of high frequency sound waves on heart muscle and other irritable
510 tissues. Am J Physiol Content 91:284–290.
511 Hynynen K, Clement G (2007) Clinical applications of focused ultrasound - The brain. Int J
512 Hyperth 23:193–202.
513 Kim H, Chiu A, Lee SD, Fischer K, Yoo SS (2014) Focused ultrasound-mediated non-invasive brain
514 stimulation: Examination of sonication parameters. Brain Stimul 7:748–756.
515 Kim H, Park MY, Lee SD, Lee W, Chiu A, Yoo SS (2015) Suppression of EEG visual-evoked
516 potentials in rats through neuromodulatory focused ultrasound. Neuroreport 26:211–215.
517 Kim H, Taghados SJ, Fischer K, Maeng LS, Park S, Yoo SS (2012) Noninvasive transcranial
518 stimulation of rat abducens nerve by focused ultrasound. Ultrasound Med Biol 38:1568–
519 1575.
520 Kleinhaus AL (1976) Divalent cations and the action potential of leech Retzius cells. Pflügers
521 Arch Eur J Physiol 363:97–104.

522 Kleinhaus AL, Prichard JW (1976) Sodium dependent tetrodotoxin-resistant action potentials in
523 a leech neuron. Brain Res 102:368–373.
524 Krasovitski B, Frenkel V, Shoham S, Kimmel E (2011) Intramembrane cavitation as a unifying
525 mechanism for ultrasound-induced bioeffects. Proc Natl Acad Sci 108:3258–3263.
526 Kubanek J, Shi J, Marsh J, Chen D, Deng C, Cui J (2016) Ultrasound modulates ion channel
527 currents. Sci Rep 6:1-14.
528 Kubanek J, Shukla P, Das A, Baccus SA, Goodman MB (2018) Ultrasound elicits behavioral
529 responses through mechanical effects on neurons and ion channels in a simple nervous
530 system. J Neurosci 38:3081–3091.
531 Lee W, Lee SD, Park MY, Foley L, Purcell-Estabrook E, Kim H, Fischer K, Maeng LS, Yoo SS (2016)
532 Image-Guided Focused Ultrasound-Mediated Regional Brain Stimulation in Sheep.
533 Ultrasound Med Biol 42:459–470.
534 Legon W, Bansal P, Tyshynsky R, Ai L, Mueller JK (2018) Transcranial focused ultrasound
535 neuromodulation of the human primary motor cortex. Sci Rep 8:1–14.
536 Legon W, Sato TF, Opitz A, Mueller J, Barbour A, Williams A, Tyler WJ (2014) Transcranial
537 focused ultrasound modulates the activity of primary somatosensory cortex in humans.
538 Nat Neurosci 17:322–329.
539 Lele PP (1963) Effects of focused ultrasonic radiation on peripheral nerve, with observations on
540 local heating. Exp Neurol 8:47–83.
541 Lin JW, Yu F, Müller WS, Ehnholm G, Okada Y (2019) Focused ultrasound transiently increases
542 membrane conductance in isolated crayfish axon. J Neurophysiol 121:480–489.
543 Menz MD, Ye P, Firouzi K, Nikoozadeh A, Pauly KB, Khuri-Yakub P, Baccus SA (2019) Radiation

Force as a Physical Mechanism for Ultrasonic Neurostimulation of the Ex Vivo Retina. J Neurosci 39:6251–6264.

Mesce KA, Newhoff M (2020) The Neural Control of Movement. In: The Neural Control of Movement, 1st ed. (Whelan PJ, Sharples SA, eds). Acedemic Press.

Min BK, Bystritsky A, Jung KI, Fischer K, Zhang Y, Maeng LS, In Park S, Chung YA, Jolesz FA, Yoo SS (2011) Focused ultrasound-mediated suppression of chemically-induced acute epileptic EEG activity. BMC Neurosci 12:23.

Muratore R, LaManna J, Szulman E, Kalisz A, Lamprecht M, Simon M, Yu Z, Xu N, Morrison B (2009) Bioeffective ultrasound at very low doses: Reversible manipulation of neuronal cell morphology and function in vitro. AIP Conf Proc 1113:25–29.

Plaksin M, Shoham S, Kimmel E (2014) Intramembrane cavitation as a predictive bio-piezoelectric mechanism for ultrasonic brain stimulation. Phys Rev X 4:011004.

Prieto ML, Firouzi K, Khuri-Yakub BT, Maduke M (2018) Activation of Piezo1 but not NaV1.2 channels by ultrasound at 43 MHz. Ultrasound Med Biol 44:1217–1232.

Puhl JG, Bigelow AW, Rue MCP, Mesce KA (2018) Functional recovery of a locomotor network after injury: plasticity beyond the central nervous system. eNeuro 5:1–16.

Qiu Z, Guo J, Kala S, Zhu J, Xian Q, Qiu W, Li G, Zhu T, Meng L, Zhang R, Chan HC, Zheng H, Sun L (2019) The mechanosensitive ion channel Piezo1 significantly mediates in vitro ultrasonic stimulation of neurons. iScience 21:448–457.

Rinaldi PC, Jones JP, Reines F, Price LRR (1991) Modification by focused ultrasound pulses of electrically evoked responses from an in vitro hippocampal preparation. Brain Res 558:36–42.

566 Sato T, Shapiro MG, Tsao DY (2018) Ultrasonic neuromodulation causes widespread cortical
567 activation via an indirect auditory mechanism. Neuron 98:1031-1041.
568 Spruston N, Johnston D (2008) Out of control in the dendrites. Nat Neurosci 11:733–734.
569 Tufail Y, Matyushov A, Baldwin N, Tauchmann ML, Georges J, Yoshihiro A, Tillery SIH, Tyler WJ
570 (2010) Transcranial pulsed ultrasound stimulates intact brain circuits. Neuron 66:681–694.
571 Tyler WJ, Tufail Y, Finsterwald M, Tauchmann ML, Olson EJ, Majestic C (2008) Remote excitation
572 of neuronal circuits using low-intensity, low-frequency ultrasound. PLoS One 3:e3511.
573 Wright CJ, Haqshenas SR, Rothwell J, Saffari N (2017) Unmyelinated peripheral nerves can be
574 stimulated in vitro using pulsed ultrasound. Ultrasound Med Biol 43:2269–2283.
575 Wright CJ, Rothwell J, Saffari N (2015) Ultrasonic stimulation of peripheral nervous tissue: An
576 investigation into mechanisms. J Phys Conf Ser 581:012003.
577 Ye J, Tang S, Meng L, Li X, Wen X, Chen S, Niu L, Li X, Qiu W, Hu H, Jiang M, Shang S, Shu Q,
578 Zheng H, Duan S, Li Y (2018) Ultrasonic Control of Neural Activity through Activation of the
579 Mechanosensitive Channel MscL. Nano Lett 18:4148–4155.
580 Yoo SH, Croce P, Margolin RW, Lee SD, Lee W (2017) Pulsed focused ultrasound changes nerve
581 conduction of earthworm giant axonal fibers. Neuroreport 28:229–233.
582 Yoo SS, Bystritsky A, Lee JH, Zhang Y, Fischer K, Min BK, McDannold NJ, Pascual-Leone A, Jolesz
583 FA (2011) Focused ultrasound modulates region-specific brain activity. Neuroimage
584 56:1267–1275.
585
586
587

Fig. 1

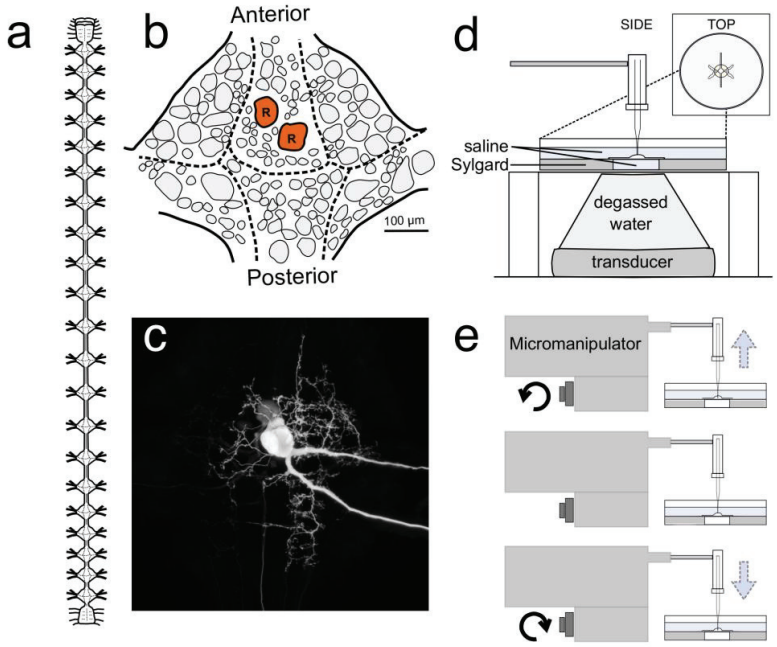


588

589

Fig. 2

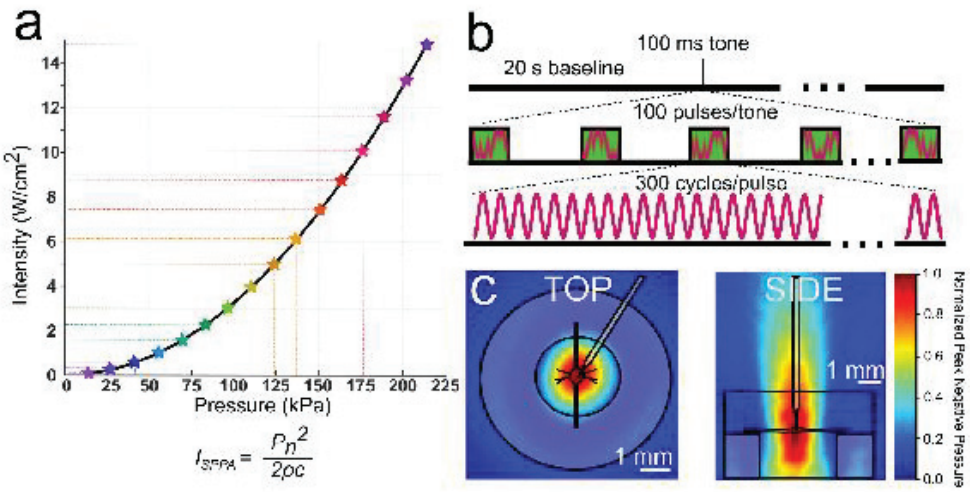


590

591

Fig. 3

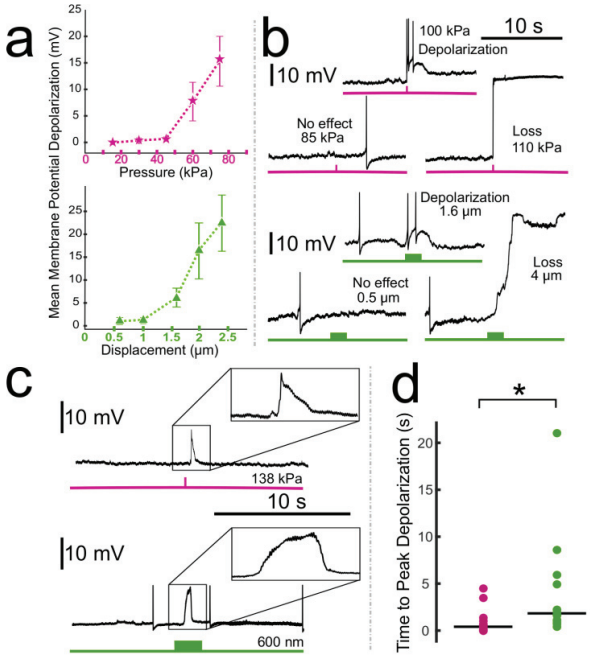


592

Fig. 4

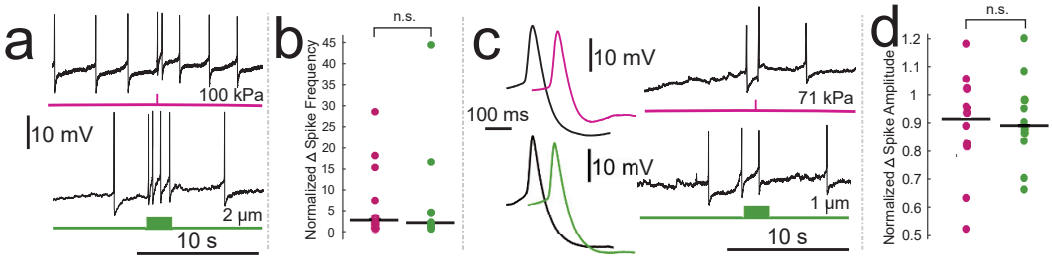

Fig. 5

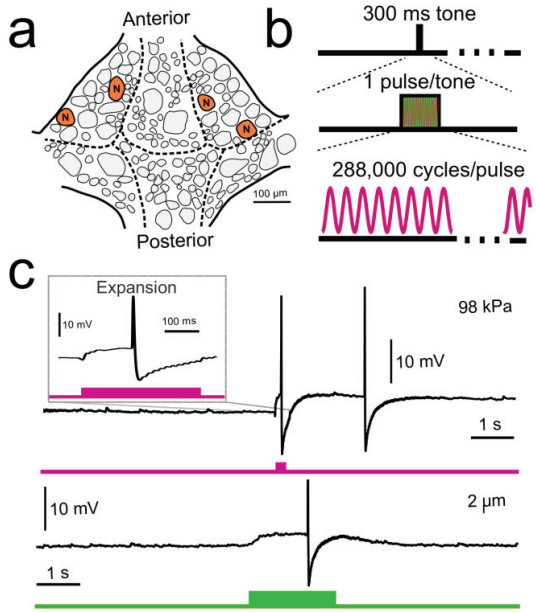


595

Fig. 6

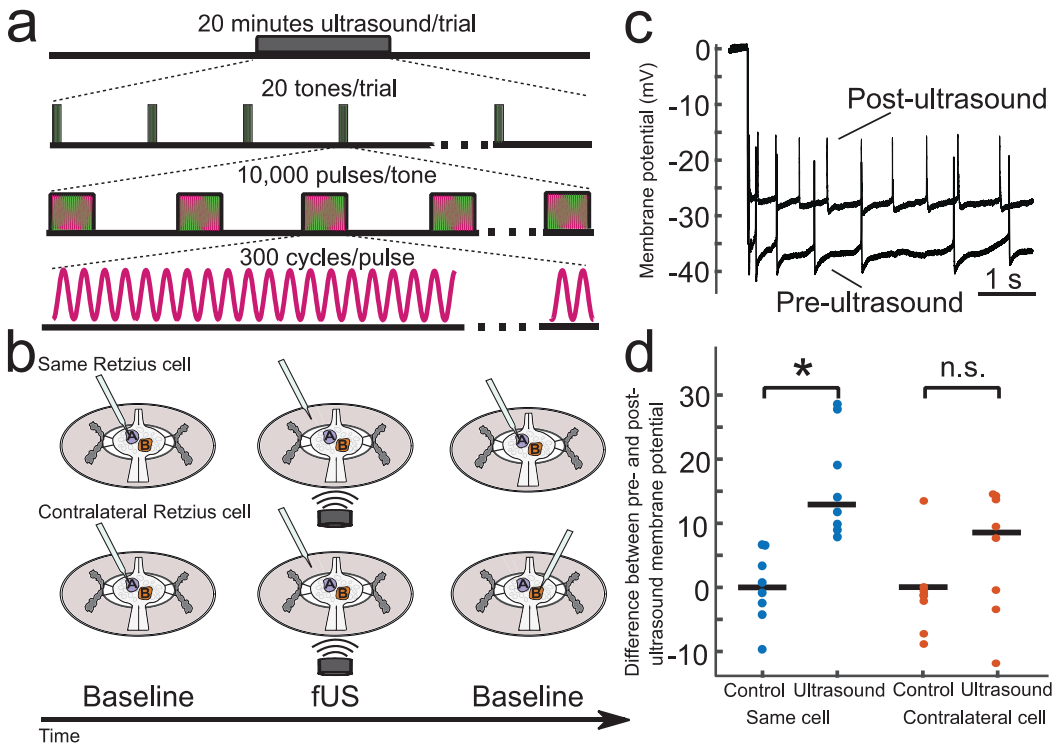


596

**FIGURE LEGENDS**

**Figure 1: The medicinal leech and experimental design**

**A.** Diagram of the central nervous system of the leech, characterized by a ventral nerve cord interspersed with 21 segmental ganglia descending from a compound cephalic ganglion. **B.** Schematic of the placement of neuronal somata on the ventral surface of a single ganglion. The bilateral Retzius cells are colored red and labeled "R". **C.** Neurobiotin fill of a Retzius cell showing its soma, neurites, and axons (a faintly labeled contralateral soma is present due to electrical coupling of the 2 cells). **D.** Ultrasound paradigm demonstrating the positioning of the transducer, intracellular electrode and ganglion preparation. **E.** Side view of the electrode displacement paradigm demonstrating the movement of the recording electrode.

**Figure 2: Ultrasound parameters**

**A.** In this graph, all the pressures utilized in this study and their corresponding intensities (spatial peak pulse average) are indicated. Intensities were calculated using the equation shown in (A) where $P_n$ = pressure; Þ = density of nerve tissue, estimated to be 1.03 g/cm$^3$; c = speed of sound in saline medium, estimated to be 1507 m/s. **B.** Ultrasound pulse parameters. 960 kHz ultrasound was applied for a single tone of 100 ms duration. Tones consisted of 100 pulses of 300 cycles of ultrasound (313 µs pulse duration). **C.** Linearly interpolated pressure distribution maps overlaid with scale preparation, dish, and electrode.

**Figure 3: Comparison of the effects of ultrasound and electrode displacement on the resting membrane potential of Retzius neurons**

**A.** Plots demonstrating changes in mean membrane potential in response to ultrasound applied at increasing pressures (upper plot, pink) and electrode displacements of increasing distance (lower plot, green), aggregated across preparations. Error bars denote standard error of the mean. **B.** Intracellular recordings demonstrating effects of ultrasound applied at increasing pressures to the same cell (pink, upper); recordings demonstrating effects of electrode displacement at increasing distances on the same cell (green, lower). **C.** Intracellular recordings demonstrating typical waveforms of depolarizations elicited by ultrasound (upper) and electrode displacement (lower). **D.** Scatter plots comparing time to peak depolarization following start of ultrasound (pink) and electrode displacement (green). Horizontal lines denote medians. The difference between the two was significant (Z= 2.6275, p=0.0086, Wilcoxon rank-sum test).

**Figure 4: Comparison of the effects of electrode displacement on the spike frequency and amplitude of Retzius neurons**

**A.** Intracellular recordings demonstrating ultrasound (upper, pink) and electrode-displacement (lower, green) associated increase in spike frequency. **B.** Scatter plots comparing the normalized change in spike frequency, during the period of peak effect, in ultrasound (pink) and electrode displacement (green) conditions. Horizontal lines denote medians. The difference between the two did not reach the threshold for significance (Z= 0.1890, p= 0.8501, Wilcoxon rank-sum test). **C.** Intracellular recordings showing that ultrasound (pink) and electrode displacement (green) induce reductions in spike amplitude. Averaged spike waveforms (left) demonstrate reduction in spike amplitude (black waveforms = averaged from the 2 spikes prior

641 to stimulus onset, pink and green waveforms = averaged from the 2 spikes fired during the peak
642 effect period following ultrasound application and electrode displacement, respectively). **D.**
643 Scatter plots comparing normalized change in spike amplitude during peak effect period in
644 ultrasound (pink) and electrode displacement (green) conditions. Horizontal lines denote
645 medians. The difference between the two did not reach the threshold for significance
646 ($t(17.3329) = 0.2777$ , $p = 0.7845$, Welch's *t*-test).
647
648 **Figure 5. Ultrasound application and electrode displacement yield similar results when a**
649 **different neuron (N cell) and different pulse parameters are used.**
650 **A.** Schematic of ventral surface of a single leech ganglion with Nociceptive (N) neurons marked.
651 **B.** Ultrasound parameters applied to N cells. We applied one tone (300 ms duration) of
652 continuous (vs. pulsed) ultrasound per trial. **C.** Representative intracellular traces of N cell
653 voltage during a trial of ultrasound application (upper, pink) and electrode displacement (lower,
654 green). When upper trace is expanded (inset), the waveform closely resembles that observed in
655 the electrode displacement paradigm. The difference in the duration of the ultrasound-induced
656 depolarization can be attributed to the difference in stimulus duration.
657
658 **Figure 6: Retzius neuron membrane potential following extended ultrasound application is**
659 **influenced by prior sharp electrode impalement**
660 **A.** Schematic of extended ultrasound application. Pulsed ultrasound was applied for a 20-
661 minute duration. Tones were delivered the first 10 seconds of each minute (tone duration = 10
662 s, tone frequency = 0.167 Hz). Tones consisted of 10,000 pulses of 300 cycles of 960 kHz

663 ultrasound (pulse repetition frequency = 1 kHz, pulse duration = 312.5 μs). Pressure applied was
664 111 kPa in all trials. **B.** Schematics of trial design for extended application paradigm. Upper:
665 Retzius neuron was impaled (blue) and resting membrane potential was recorded. The
666 recording electrode was then removed (middle cartoon) and ultrasound was applied for 20
667 minutes. Following ultrasound application, the electrode was re-inserted into the same Retzius
668 cell for a second baseline recording. Lower: In a different preparation, the electrode was
669 inserted into the Retzius cell (blue) to record the resting membrane potential. As in the
670 previous experiment, the electrode was removed prior to 20 minutes of ultrasound application
671 (middle cartoon). After application, the contralateral Retzius cell (orange) was impaled to
672 record baseline activity; this cell was thus not previously impaled. **C.** Intracellular recordings
673 taken from the same Retzius cell before and after extended application of ultrasound
674 demonstrating post-ultrasound depolarization of the resting membrane potential. **D.** Scatter
675 plots comparing differences between pre- and post-ultrasound membrane potential in the
676 same cell (blue) and contralateral cell (orange). Control paradigms replaced the ultrasound
677 application period with a waiting period of equivalent time. Membrane potentials of the
678 ultrasound-treated and control groups differed significantly (Wilcoxon rank-sum test, p = 1.55e-
679 4) when the same Retzius cell was re-impaled. However, the ultrasound and control groups did
680 not differ significantly (Wilcoxon rank-sum test, p = 0.1605) when the contralateral cell was
681 recorded.
682
683 **Table 1: Descriptions of statistical tests.**

684 Letters (leftmost column) correspond to p-values of statistical tests as reported in Results. The
685 data structure, test type, result, effect size, and statistical power of these tests are described.
686 Results of Shapiro-Wilk test for normality of data in ultrasound (US) and electrode displacement
687 (ED) conditions ($\alpha$=0.05) are reported under "Data Structure." Normally distributed data were
688 compared with Welch's *t* test, and non-normal data were compared with the nonparametric
689 Wilcoxon rank-sum test. Effect sizes were calculated as Cohen's d with correction for small
690 sample sizes as described by Durlak (2009).
691